microRNA-seq of cartilage reveals an over-abundance of miR-140-3p which contains functional isomiRs

Steven Woods[1], Sarah Charlton[2], Kat Cheung[2], Yao Hao[2,3], Jamie Soul[2], Louise N Reynard[2], Natalie Crowe[4], Tracey E. Swingler[4], Andrew J. Skelton[2], Katarzyna A. Piróg[2], Colin G. Miles[2], Dimitra Tsompani[2], Robert M. Jackson[2], Tamas Dalmay[4], Ian M. Clark[4], Matt J. Barter[2], David A. Young[2]*

[1]Division of Cell Matrix Biology and Regenerative Medicine, Faculty of Biology Medicine and Health, University of Manchester, Michael Smith Building, Oxford Road, Manchester, M13 9PT, UK
[2]Skeletal Research Group, Biosciences Institute, Newcastle University, Central Parkway, Newcastle upon Tyne, NE1 3BZ, UK
[3]Orthopedics Department, First Hospital of Shanxi Medical University, Yingze District, Taiyuan, 030000, China
[4]School of Biological Sciences, University of East Anglia, Norwich, NR4 7TJ, UK
*To whom correspondence should be addressed. Tel: +44 191 2418831; FAX: Not applicable; Email: david.young@ncl.ac.uk

ABSTRACT

MiR-140 is selectively expressed in cartilage. Deletion of the entire miR-140 locus in mice results in growth retardation and early-onset osteoarthritis-like pathology, however the relative contribution of miR-140-5p or miR-140-3p to the phenotype remains to be determined. An unbiased small RNA sequencing approach identified miR-140-3p as significantly more abundant (>10-fold) than miR-140-5p in human cartilage. Analysis of these data identified multiple miR-140-3p isomiRs differing from the miRBase annotation at both the 5′ and 3′ end, with >99% having one of two seed sequences (5′ bases 2-8). Canonical (miR-140-3p.2) and shifted (miR-140-3p.1) seed isomiRs were overexpressed in chondrocytes and transcriptomics performed to identify targets. miR-140-3p.1 and miR-140-3p.2 significantly downregulated 694 and 238 genes respectively, of which only 162 genes were commonly downregulated. IsomiR targets were validated using 3 ′UTR luciferase assays. miR-140-3p.1 targets were enriched within upregulated genes in rib chondrocytes of *Mir140*-null mice and within downregulated genes during human chondrogenesis. Finally, through imputing the expression of miR-140 from the expression of the host gene *WWP2* in 124 previously published datasets, an inverse correlation with miR-140-3p.1 predicted targets was identified. Together these data suggest the novel seed containing isomiR miR-140-3p.1 is more functional than original consensus miR-140-3p seed containing isomiR.

INTRODUCTION

MicroRNAs (miRNAs) are small non-coding RNAs that regulate gene expression. Mature miRNAs are processed from primary transcripts containing stem loops by cleavage mediated by Drosha and then Dicer proteins (Bartel 2004). The 5′ and 3′ sides of the stem loop can both give rise to mature miRNAs termed ′-5p′ and ′-3p′ respectively (Griffiths-Jones 2004). These mature miRNAs are then loaded into the RNA-induced silencing complex (RISC) to mediate either mRNA degradation or translation inhibition of target mRNA through binding of the miRNA seed sequence (5′ bases 2-8) to the target 3′UTR (Bartel 2009). The level of complementarity between the seed and target mRNA is important for target repression. Binding to positions 2-7 of the miRNA may indicate target repression, however either an adenine binding to position 1 of the miRNA (7a1 targets), a match at position 8 (7m8 targets) or both (8mer targets) can improve target repression (Lewis et al. 2005).

In recent years, small RNA (sRNA) sequencing (sRNA-seq) has identified additional miRNAs that do not perfectly align to the annotated mature miRNA, known as isomiRs (Morin et al. 2008). IsomiRs may be shorter or longer at the 5′ and/or 3′ end of the mature miRNA, and are not always templated to the genomic DNA. Variants at the 3′ end are quite common, although not thought to alter the miRNA target repertoire (Wyman et al. 2011). Variations at the 5′ end are less common but are of greater importance due to altered seed sequence, target repertoire and potentially the function of miRNAs. The type of 5′isomiR variation is critical for determining the consequence on target repertoire, for example 5’ isomiRs of microRNAs can have highly over-lapping (Cloonan et al. 2011; Llorens et al. 2013) or divergent (Tan et al. 2014) targets, which is dependent upon the presence or absence of a uracil (U) at position 2 of the longer sequence (Manzano et al. 2015).

The most studied miRNA in cartilage is miR-140, which produces miR-140-5p and miR-140-3p (Wienholds et al. 2005; Miyaki et al. 2009; Miyaki et al. 2010). Deletion of *Mir140* in mice leads to a skeletal phenotype including an osteoarthritis (OA)-like disease. Although the contribution of the lack of miR-140-5p or miR-140-3p to the phenotype remains largely undetermined, the majority of studies have focused on miR-140-5p rather than miR-140-3p (Wienholds et al. 2005; Miyaki et al. 2009; Miyaki et al. 2010), with the reason behind this -5p bias unclear. Barter *et al*. showed a particularly important role for miR-140-5p during human chondrogenesis with many genes under its control, and although they used a systematic approach, they did not include isomiRs within their analysis (Barter et al. 2015). miR-140-3p is less well studied than miR-140-5p and only a small number of -3p targets have been identified, which so far appear to have little relevance to cartilage and OA. Intriguingly, using small RNA sequencing (sRNA-seq) of human cartilage RNA we identified that miR-140-3p was high in abundance (>10-fold) compared to miR-140-5p (Crowe et al. 2016).

Although there have been several studies to elucidate the role of miRNAs in cartilage and chondrogenesis, the role of isomiRs has been largely ignored. Here we show miR-140-3p

isomiRs are abundantly expressed in cartilage and that these isomiRs are present in RISC. Using over expression followed by transcriptomic analysis we show two miR-140-3p isomiRs (miR-140-3p.1 and miR-140-3p.2) have largely discrete target repertoires. We validated a number of common and discrete targets for each isomiR using a luciferase reporter system. We present evidence that miR-140-3p.1, which is not currently annotated in miRBase, may play roles in human chondrogenesis, mouse cartilage and in multiple other skeletal tissues.

MATERIAL AND METHODS

Analysis of cartilage sRNA-seq

sRNA-seq was analysed as previously described (Sorefan et al. 2012; Crowe et al. 2016). 5′ isomiRs were defined using the following criteria: 1) loss or gain of 1 or more nucleotides, using the mature miRBase (release 22.1) (Kozomara and Griffiths-Jones 2011) sequences as a reference; 2) a read count >100, and 3) a read count > 5% of the mature miRBase reference sequence for that miRNA.

Analysis of non-cartilage sRNA-seq

Read count for non-cartilage sRNA-seq including; melanoma (Stark *et al*. 2010 (Stark et al. 2010)), cervix (Witten *et al*. 2010 (Witten et al. 2010)), lymphocytes (Kuchen *et al*. 2010 (Kuchen et al. 2010)) was obtained from miRBase (Kozomara and Griffiths-Jones 2011), or directly from publication for sRNA-seq following immunoprecipitation of Argonaute (AGO) proteins (Burroughs *et al*. (Burroughs et al. 2011)). Sequences were designated as either miR-140-3p.1 or miR-140-3p.2 based upon seed sequence. For the analysis, mouse cortex CLEAR (covalent ligation of endogenous Argonaute-bound RNAs)-CLIP data (NCBI GEO GSE73059) was analysed as previously described (Moore et al. 2015) using the parameters provided. Briefly, the reads were quality filtered, duplicate reads collapsed, trimmed and the barcodes stripped using the CLIP Tool kit (Shah et al. 2017). The TargetScanMouse 7.2 miRNA database was mapped against each sample (treated as a reference genome) using Bowtie (v1.0.0). miRNA-first chimeric reads uniquely assignable to the miR-140 isomiRs were identified in R, potential PCR duplicates with the same degenerate barcode were collapsed and filtered to retain reads with chimeric mRNA sequences >20nt in length.

Human articular chondrocyte isolation, culture and transfection

Human articular chondrocyte isolation from knee cartilage was performed as previously described (Barter et al. 2015). Tissue was donated by patients with diagnosed osteoarthritis and undergoing joint replacement surgery, with informed consent and ethics committee approval. Briefly, macroscopically normal cartilage was removed from the subchondral bone and dissected into ~1mm pieces using scalpel and forceps. Enzymatic digestion was performed using trypsin and then collagenase overnight at 37^{o}C. Chondrocytes were then grown to confluence and plated into 6 well plates for miRNA/isomiR mimic transfection. 100nM miRNA mimic and control were transfected into HAC using DharmaFECT 1 transfection reagent (Dharmacon, Horizon Discovery, Cambridge, UK) according to the manufacturer's protocol and essentially as previously described (Barter et al. 2015). 48h post-transfection HAC were lysed and RNA harvested using Qiagen miRNeasy kit (Qiagen, Crawley, UK). Custom miRNA mimics with each isomiR sequence were purchased from Dharmacon, standard (A4) desalted purification.

Microarray and identification of targets in human chondrocytes

Microarray was performed by Cardiff University, Central Biotechnology Services, using Illumina whole-genome expression array Human HT-12 V4 (Illumina, Saffron Walden, U.K.). Normalization of the quantified signals (background corrected) was performed using the global Lowess regression algorithm. Expression analysis was performed in R/bioconductor using the limma package (Smyth 2004). PCA and heat map were generated using ClustVis (Metsalu and Vilo 2015). PCA analysis was performed on normalised expression values of all unique genes detected by the microarray analysis. Data was not transformed; row scaling was unit variance and the PCA method selected was singular value decomposition (SVD) with computation. Heat map is based on the top 650 significant genes for each comparison (miC vs. mR-140-3p.1 or miC vs. miR-140-3p.2), which after removal of duplicates gave 882 genes in total. Clustered distance was based on correlation with the method set to average. TargetScanHuman (version 7.2 (Agarwal et al. 2015a)) was used to predict targets of miR-140-3p.1 and miR-140-3p.2. In order to demonstrate discrete functions we investigated unique targets for each isomiR (3p.2 and 5p targets were removed from 3p.1 analysis; 3p.1 and 5p targets were removed from 3p.1 analysis; 3p.1 and 3p.2 targets were removed from 5p analysis). Genes were selected for luciferase validation based on both altered expression in miR-140-3p.1 or miR-140-3p.2 transfected cells versus control and on expression in miR-140-3p.1 transfected cells versus expression in miR-140-3p.2 transfected cells.

Target enrichment and pathway analysis

Sylamer analysis was performed on ordered gene lists from most downregulated to most upregulated (including genes whose expression did not significantly change) (van Dongen et al. 2008). Target enrichment (%targets) was calculated by dividing the total number of predicted targets (TargetScan 7.2) that significantly increased or decreased by the total number of genes that significantly increased or decreased, multiplied by 100. Cumulative fraction plots were generated as previously described (Woods et al. 2019), using ordered gene list from downregulated to most upregulated (regardless of significance) and predicted targets from TargetScan 7.2. Pathway analysis was performed using Database for Annotation, Visualization and Integrated Discovery (DAVID) v6.7(Huang da et al. 2009) and g-Profiler (Raudvere et al. 2019).

Q-RT-PCR for miR-140-3p.1 and miR-140-3p.2

Custom miR-140-3p.1 and miR-140-3p.2 assays (Exiqon, Qiagen, Aarhus, Denmark) were used to detect expression of miR-140-3p.1 and miR-140-3p.2. Assays were validated using spike-in of miR-140-3p.1 and miR-140-3p.2 mimic (Dharmacon).

3′UTR luciferase reporter construction and assay

In-Fusion® cloning (Clontech, Takara Bio Europe SAS, Saint-Germain-en-Laye, France) of selected 3′UTRs into the pmirGLO vector (Promega, Southampton, UK) was used to generate 3′UTR luciferase reporters essentially as previously described (Barter et al. 2015) (Supplementary Table 10). SW1353 chondrosarcoma cells were seeded and cultured to

reach ~50% confluence after 24 h (Barter et al. 2015). miRNA (100 nM) were transfected using DharmaFECT 1 transfection reagent, reporter plasmids (500 ng/ml) were transfected using FugeneHD (Promega). 24h after transfection luciferase levels determined using Promega dual luciferase assay and GloMax plate reader (Promega).

Generation of miR-140$^{-/-}$ mice

All animal experiments were performed under licenses granted from the Home Office (United Kingdom) in accordance with the guidelines and regulations for the care and use of laboratory animals outlined by the Animals (Scientific Procedures) Act 1986 according to Directive 2010/63/EU of the European Parliament, and conducted according to protocols approved by the Animal Ethics Committee of Newcastle University and the Home Office, United Kingdom. Post-generation breeding and subsequent phenotyping were performed under licences PPL60/4525 and P8A8B649A. CRISPR/Cas9 guide RNAs (crRNA) were designed using CHOPCHOP. crRNA linked with TRACR (sgRNA) were amplified by PCR with a pLKO vector (Addgene_52628) as template, using the primer T7 TRACR R (Supplementary Table 10) and a 5′ PCR primer that included a T7 sequence and the crRNA. This was converted to RNA using the MEGAshortscript T7 kit (Fisher Scientific). sgRNA (50ng/ml each) were mixed with recombinant Cas9 (ToolGen, CamBioScience Limited, Cambridge, UK) and injected into the cytoplasm of donor mouse zygotes and transferred into recipient foster mothers, all essentially as previously described (Ittner and Gotz 2007; Ran et al. 2013; Yang et al. 2013). The mixed C57BL/6 and CBA/ca F_0 mice were backcrossed onto C57BL/6J and heterozygous animals crossed three times to eventually generate wild-type and null lines used in purification of rib chondrocytes. Genotype was confirmed by ear-notch PCR and Sanger sequencing (Supplementary Figure S5).

Mouse rib chondrocyte isolation and RNA-seq

Primary mouse costal chondrocytes were isolated from 7-day-old miR-140$^{-/-}$ and wild-type (WT) mice using collagenase digestion, essentially as previously described (Grigelioniene et al. 2019a). Total RNA, including miRNA was isolated using the miRVana miRNA Isolation Kit (with phenol)(Fisher Scientific). Sequencing libraries were prepared from 500 ng of purified total RNA using the Illumina TruSeq Stranded mRNA sample preparation kit according to the manufacturer's protocol, and sequenced on Illumina NextSeq500. Each sample provided >12 million single-end 75-bp sequencing reads. Sequenced reads were mapped to the mm10 transcriptome using Salmon (Patro et al. 2017). Batch effects were estimated using RUVseq (Risso et al. 2014) and incorporated into the differential expression analysis performed using DESeq2 (Love et al. 2014). PCA and heat map were generated using ClustVis (Metsalu and Vilo 2015) using the parameters defined above, using all transcripts for the PCA and the top 1200 significant transcripts based on p-value for the heatmap.

Analysis of human MSC chondrogenesis

Microarray data of human MSC chondrogenesis was previously published by Barter *et el.* (Barter et al. 2015). Data was re-analysed for changes in expression of miR-140-3p.1 and miR-140-3p.2 predicted targets, lists of conserved predicted targets were obtained from TargetScan (version 7.2). Enrichment for 7m8 seed sequence binding sites was performed using Sylamer (van Dongen et al. 2008).

SkeletalVis analysis

Gene expression responses within SkeletalVis were filtered for human and mouse data sets and where *WWP2* expression significantly changed (adjusted p-value is <0.05, no fold change cut off), leaving 124 experimental comparisons. The change in *WWP2* expression was plotted against the average fold change of predicted (TargetScan7.2) miRNA targets for each experimental comparison. Correlation (R^2) and regression analysis for all 124 experimental comparisons was calculated using the data analysis add-in in Microsoft Excel. The percentage (% of miRNA targets) was calculated by dividing the total number of predicted targets (TargetScan 7.2) that significantly increased or decreased by the total number of genes that significantly increased or decreased, multiplied by 100, for each of the 124 experimental comparisons. The percentage of miR-140-5p, miR-140-3p.1 and miR-140-3p.2predicted targets within up-, no change or downregulated genes was then plotted against log2 FC for *WWP2*, the trend lines represent the cumulative mean starting from studies where *WWP2* is most up- or downregulated to studies where *WWP2* changes least, to demonstrate trend. A list of randomly generated genes was analysed alongside miR-140-5p, miR-140-3p.1 and miR-140-3p.2. 'Targets Enrichment (up/down)' was calculated by dividing the '% of miRNA targets within up-regulate genes' by the '% of miRNA targets within downregulated genes', this was performed for each miRNA in each study. The mean 'Target enrichment (up/down)' for studies where *WWP2* either decreased or increased was plotted. 'Targets Enrichment (up/down)' for miR-140-5p, miR-140-3p.1 and miR-140-3p.2 predicted targets was also plotted against each other. Experimental comparisons where *WWP2* decreased or increased were shown in different colours as described.

RESULTS

RNA-Seq of articular cartilage identifies an overabundance of miR-140-3p and miR-140-3p isomiRs

We performed sRNA-seq of human cartilage RNA and identified novel cartilage specific miRNAs (Crowe et al. 2016). Our cartilage sRNA-seq aligned to 990 miRNAs annotated in miRBase (Kozomara and Griffiths-Jones 2011), 704 of which contained at least one additional type of potential isomiR (Supplemental Table S1). As 5′ isomiRs are most likely to alter function, we focused further sRNA-seq analysis on miRNAs with 5′isomiRs. Using thresholds of >100 reads and >5% of total reads for that miRNA, we identified 5′isomiR sequences for 29 miRNAs, 26 of which have a single addition (includes templated and non-templated additions) or deletion at the 5′ nucleotide, while miR-3074-5p, miR-455-3p and let-7b-3p all have two additional 5′ nucleotides (Supplemental Figure S1). Although the isomiR for miR-1246 is just under our read threshold (read count of 99), it appears to have four additional 5′ nucleotides compared to the miRBase annotation (Supplemental Figure S1).

MiR-140-3p and its isomiRs account for more than half of all sequencing reads in our cartilage sRNA-seq (Figure 1A). As miR-140 is the most studied cartilage miRNA, yet most attention has been paid to miR-140-5p, this report will focus on mirR-140-3p and its isomiRs. IsomiRs can be sub-divided into several categories, essentially either templated or non-templated with either 5′ or 3′ modifications (Cloonan et al. 2011). miR-140-3p isomiRs are predominantly 3′ additions and mixed type isomiRs, with only 5% aligning to the original miRBase annotation (Figure 1B). More than 99% of all miR-140-3p isomiRs result in one of two seed sequences; ACCACAG as annotated in miRBase, and CCACAGG, which is shifted by -1 nucleotide (shifted by one nucleotide in the 3′ direction) (Figure 1C). Twenty-five percent of reads for miR-140-3p were perfectly templated to DNA (Figure 1D), the remainder contained one or more non-templated nucleotides, predominantly non-templated 3′ adenine additions (Figure 1E), which were observed in sequencing reads containing both of the seed sequences (Figure 1F and G). The most detected isomiR with each seed are termed miR-140-3p.1 (ACCACAGGGTAGAACCACGGAC, seed CCACAGG) and miR-140-3p.2 (TACCACAGGGTAGAACCACGGA seed: ACCACAG), respectively (Figure 1H). Expression of miR-140-3p.1 and miR-140-3p.2 in cartilage (performed with a 2-fold serial dilution) was validated using qRT-PCR with isomiR selective assays (Figure 1I).

Analysis of other published sRNA-seq data identified the presence of miR-140-3p.1 and miR-140-3p.2 in other human tissue types, although expressed at a lower level than in cartilage (Supplemental Figure S2) (Kuchen et al. 2010; Stark et al. 2010; Witten et al. 2010). As miRNA bound to Argonaute (AGO) indicates the ability to repress targets (Flores et al. 2014), we analysed sRNA-seq data following immunoprecipitation of AGO proteins (Burroughs et al. 2011). Indeed, both miR-140-3p.1 and miR-140-3p.2 were present (RISC; Supplemental figure S2). Furthermore analysis of CLEAR-CLIP, a modified version of high-throughput

sequencing of RNA isolated by crosslinking immunoprecipitation (HITS-CLIP), from mouse brain (Moore et al. 2015), identified sequences corresponding to both miR-140-3p.1 and miR-140-3p.2 ligated to endogenous mRNA potential targets (Supplemental Figure S2). Together these data indicate miR-140-3p.1 and miR-140-3p.2 can be loaded into RNA-induced silencing complex and can target transcripts.

miR-140-3p.1 and miR-140-3p.2 are predicted to have distinct targets

miRNAs generally target mRNAs through interaction of their seed sequence (nucleotides 2-7), the seed sequences for miR-140-3p.1 and miR-140-3p.2 differ (CCACAGG and ACCACAG, respectively; Figure 2A). Thus, each miR-140-3p isomiR has different preferences for seed binding sites (Figure 2A). Indeed, target prediction analysis for miR-140-3p.1 and miR-140-3p.2 by TargetScan 7.2 (conserved) identifies only 133 shared targets, a small number compared to the total number of predicted targets (665 and 495 for miR-140-3p.1 and miR-140-3p.2, respectively, Figure 2B, Supplemental Table S2). The majority of these targets also differ from predicted miR-140-5p targets (Figure 2B, Supplemental Table S2).

Identification and validation of miR-140-3p.1 and miR-140-3p.2 targets in human chondrocytes

Next, we used overexpression of miR-140-3p.1 and miR-140-3p.2 in primary human chondrocytes followed by genome-wide transcriptomics to experimentally identify similarities and differences in their target repertoire. Overexpression of miR-140-3p.1 and miR-140-3p.2 was validated using isomiR-specific qRT-PCR (Figure 3A). Principal component analysis (PCA) and heat map illustrated clustering of biological replicates and differences between miR-140-3p.1 and miR-140-3p.2 in transfected chondrocytes (Figure 3B and C). 693 and 237 genes were significantly (adjusted p-value<0.05) downregulated by miR-140-3p.1 and miR-140-3p.2 respectively, however only 161 genes were commonly downregulated by both isomiRs (compared to control; Figure 3D, Supplemental Table S3, Supplemental Table S4). DAVID pathway analysis of repressed genes identified enrichment terms associated with 'phosphoprotein' for miR-140-3p.1 (Supplemental Table S5). Direct comparison of miR-140-3p.1 transfected with miR-140-3p.2 transfected cells revealed 237 genes were significantly different between the two isomiRs (Supplemental Table S3, Supplemental Table S4). DAVID pathway analysis of the 237 genes differentially expressed between the two isomiRs identified an enrichment of triple helical collagen genes (*COL2A1, COL4A1, COL6A3, COL11A1, COL11A2*; p=0.0004, adjusted p-value=0.066; Supplemental Table S5). Similarly, g-Profiler analysis of genes differentially expressed between miR-140-3p.1 and miR-140-3p.2 transfected chondrocytes, revealed an enrichment of genes associated with ECM structure including 'connective tissue development' (adjusted p-value 0.005; Supplemental Figure S3). The fraction of these genes that are decreased by, and are predicted to be a targets of each isomiR, is greater for miR-140-3p.1 than for miR-140-3p.2, suggesting miR-140-3p.1 directly regulates genes belonging to these terms. However, the majority of genes contributing to the enrichment are not predicted direct targets of either miR-140-3p.1 or miR-140-3p.2,

suggesting miR-140-3p isomiRs, in the most part, regulate these processes through indirect mechanisms. Together these data indicate that the sequence differences between the two isomiRs may be functionally important.

Sylamer, a non-bias motif analysis tool, was used to investigate miRNA binding site enrichment within downregulated 3′UTRs (van Dongen et al. 2008). Transfection of either miR-140-3p.1 or miR-140-3p.2, showed specific enrichment for 8mer, 7m8, 7a1 and 6mer seed binding sites of the transfected isomiR. Interestingly, a greater enrichment was observed for miR-140-3p.1 (non-canonical seed) binding sites than miR-140-3p.2 (canonical seed) binding sites (Figure 3E). Predicted targets (identified using TargetScan 7.2) that are unique to either miR-140-3p.1 or miR-140-3p.2 were downregulated following overexpression of either miR-140-3p.1 or miR-140-3p.2 respectively, but not downregulated by the reciprocal isomiR (Figure 3F), suggesting both isomiRs can repress specific transcripts in human chondrocytes.

Based upon expression of individual genes (Supplemental Table S3), unique and common targets were then selected for 3′UTR luciferase validation (Figure 3G-I). As expected *LIPA*, *RCL1*, *COL4A1* and *SLC35D2* were validated as miR-140-3p.1 targets; *NUDT21*, *REEP5* and *SDC4* were validated as miR-140-3p.2 targets and *PAX2* validated as a target of both miR-140-3p.1 and miR-140-3p.2. Interestingly, the *REEP5* 3′UTR luciferase construct was also repressed by miR-140-3p.1, although not a predicted target of miR-140-3p.1. Conversely, *DAAM1* and *ALDH1A3* are predicted targets of both miR-140-3p.1 and miR-140-3p.2, however significant repression was only observed for miR-140-3p.1 and not for miR-140-3p.2. Contrary to the repression role of miRNAs in gene regulation, miR-140-3p.1 increased luciferase for the *MARCKSL1*, *KIAA1199* and *MAPILC3A* 3′UTR reporters.

miR-140-3p isomiRs are functional in mouse cartilage

Analysis of mouse sRNA-Seq data revealed that both miR-140-3p.1 and miR-140-3p.2 are present (Figure 4A-C) and more abundant than miR-140-5p (Chiang et al. 2010) (Supplemental Figure S4A), indicating miR-140-3p 5′ isomiRs are conserved across species, although there are some differences in abundance of 3′ variations. We and others have generated *Mir140*-null mice, which lack all miRNAs and isomiRs produced from the *Mir140* locus (Supplemental Figure S5). Transcriptome RNAseq data of rib cartilage from these mice identified 1894 and 1179 genes that were significantly up and downregulated respectively (Supplemental Table S6, Supplemental Table S7). Pathway analysis of upregulated genes following knock out (KO) of *Mir140* identified terms associated with ‘phosphoprotein’ (Supplemental Table S8), which is consistent with pathway analysis of genes decreased following miR-140-3p.1 overexpression in human chondrocytes (Supplemental Table S5). miR-140-5p, miR-140-3p.1 and miR-140-3p.2 predicted targets (identified using TargetScan 7.2) were enriched within upregulated genes (Figure 4D), and their average expression increased following KO of the *Mir140* locus (Figure 4E), indicating a loss of target repression.

Furthermore, cumulative fraction plot analysis indicates that the fraction of targets that decrease following KO of the *Mir140* locus is lower than expected (Figure 4F). Non-biased Sylamer analysis also identified an enrichment of miR-140-5p, miR-140-3p.1 and miR-140-3p.2 7m8 seed binding sites within upregulated genes; miR-140-5p displayed the greatest enrichment, followed by miR-140-3p.1 and then miR-140-3p.2 (Figure 4G).

More than 99% of miRNAs produced from the murine *Mir140* locus share seed binding sites with either miR-140-5p, miR-140-3p.1 or miR-140-3p.2; of these miR-140-5p has the lowest read count, yet has the largest contribution to target repression (Figure 4). We used Sylamer to investigate the possibility that other lowly expressed sequences produced from the *Mir140* stem loop (Supplemental Figure S4A), may contribute to target repression. This analysis indicates miR-140-5p followed by miR-140-3p.1 have the largest contribution to target repression in mir140 KO mice (Supplemental Figure S4B), and that there are no lowly expressed *Mir140*-derived miRNAs that have a major contribution to target repression in mice.

miR-140-3p.1 targets are enriched within downregulated genes during MSC chondrogenesis

miR-140 is highly upregulated during mesenchymal stem cell (MSC) chondrogenesis, with miR-140-5p predicted targets highly enriched within the downregulated genes (Barter et al. 2015). Here we show through re-analysis of this transcriptomic dataset (Figure 5A) that expression of predicted targets of both miR-140-3p.1 and miR-140-3p.2 are decreased during chondrogenesis. Similar to miR-140-5p predicted targets, the average expression of miR-140-3p.1 and miR-140-3p.2 predicted targets decreased during chondrogenesis, with unique miR-140-3p.1 targets being more repressed than unique miR-140-3p.2 predicted targets ($p=0.07$) (Figure 5B). Sylamer analysis indicated enrichment for miR-140-5p and miR-140-3p.1, but minimal enrichment for miR-140-3p.2 (Figure 5C). Consistent with *Mir140* null mouse data, the enrichment of miR-140-5p was greater than for both miR-140-3p.1 and miR-140-3p.2 in genes whose expression decreased during human MSC chondrogenesis (Figure 5C).

miR-140-5p and miR-140-3p.1 predicted targets inversely correlate with *WWP2* in multiple skeletal tissues

Having established miR-140-5p, miR-140-3p.1 and miR-140-3p.2 targets are regulated during human MSC chondrogenesis and in mouse rib chondrocyte development, we next looked for evidence of an inverse correlation between miR-140 and target gene expression in other skeletal tissues. Whole genome transcriptomic datasets of skeletal tissues following various perturbations have been collated within SkeletalVis, a data portal for cross-species skeletal transcriptomics data (Soul et al. 2018). Although the majority of these studies do not directly assess miRNA expression, miRNAs that are located in the introns of protein coding genes, including miR-140, and are frequently co-regulated with their host gene

(Franca et al. 2016). A number of studies have utilised host-gene expression to predict the gene targets of intronic miRNAs through a consistent negative correlation in expression (Gennarino et al. 2009; Radfar et al. 2011). miR-140 is located in intron 16 of *WWP2*, with expression of the miR and an abundant isoform of *WWP2* (transcript variant 2) controlled by a common promoter (Yamashita et al. 2012). *WWP2* was therefore used as a surrogate for miR-140 expression.

Of the 779 skeletal gene expression responses within SkeletalVis, 124 contained a significant alteration (adjusted p-value <0.05, no fold change cut off) in *WWP2* expression. The change in *WWP2* expression (as a surrogate for miR-140 expression) was plotted against the average fold change of predicted miRNA isomiR targets for each study. Using regression analysis we identified a significant inverse relationship between *WWP2* and miR-140-5p (Figure 6A; r^2=0.38, p=3.08x10^{-14}) and miR-140-3p.1, predicted targets (Figure 6B; r^2=0.16, p=5.46x10^{-6}). There was a minimal inverse relationship between *WWP2* and miR-140-3p.2 predicted targets (Figure 6C; r^2=0.05, p=0.012) or randomly selected genes (Figure 6D). We then divided the studies into two; those where *WWP2* significantly decreased and those where *WWP2* significantly increased. The average target log2FC of predicted miR-140-5p, miR-140-3p.1 and miR-140-3p.2 targets was significantly higher in studies where *WWP2* decreased than studies where *WWP2* increased (Supplemental Figure S6A). To determine if miR-140-5p, miR-140-3p.1 and miR-140-3p.2 targets are regulated in a similar way in each study, we correlated log2FC for miR-140-5p, miR-140-3p.1 and miR-140-3p.2 targets for all studies (Supplemental Figure S6B). Average log2FC for miR-140-5p targets correlated most strongly with average log2FC for miR-140-3p.1 targets (Supplemental Figure S6B). The direction of target FC tends to be in the opposite direction to WWP2 FC (Supplemental Figure S6B). Thus, where *WWP2* expression changes the expression of predicted miR-140 targets have a tendency to change in the opposite direction.

In addition to average log2FC of predicted targets, we also investigated the percentage of predicted targets that increased or decreased within each of the studies. Within studies where *WWP2* expression increased there was generally a larger percentage of predicted miR-140-5p and miR-140-3p.1 targets within downregulated genes than within upregulated genes, this was not true for miR-140-3p.2 (Figure 6E-H). For the contrary, when *WWP2* expression decreased, there was generally a larger percentage of miR-140-5p targets within upregulated genes than within downregulated genes, however there was little evidence of this for miR-140-3p.1 or miR-140-3p.2(Figure 6E-H). Within *Mir140* null mice (large symbols), where *WWP2* expression was not altered, the percentage of targets within the upregulated genes is greater than the percentage of targets within downregulated genes (Figure 6E-H).

Next we calculated 'Target Enrichment (up/down)' by dividing the percentage of targets within upregulated genes by those within the downregulated genes, for each of the studies

(a value >1 indicates more targets within upregulated whereas a value <1 indicates more targets within downregulated genes). Target enrichment for miR-140-5p and miR-140-3p.1 was significantly higher in studies where *WWP2* decreased than in studies where *WWP2* increased (Supplemental Figure S6C). Similar to the log2FC analysis, the enrichment for miR-140-5p targets correlated most strongly with enrichment for miR-140-3p.1 targets (Supplemental Figure S6D).

These data indicate that when *WWP2* expression increases, both miR-140-5p and miR-140-3p.1 predicted targets are repressed. Furthermore, they also indicate that miR-140-3p.2, which contains the miRBase annotated seed sequence, has a less significant biological effect on gene expression than either miR-140-5p or miR-140-3p.1.

To further refine prediction of putative direct miR-140 targets, we investigated the overlap between four criteria; TargetScan predicted targets, genes downregulated following overexpression in human chondrocytes, genes upregulated in mice lacking the *Mir140* locus, and genes upregulated during MSC chondrogenesis. There were 3, 3 and 0 genes matching all of these criteria for miR-140-5p, miR-140-3p.1 and miR-140-3p.2, respectively (Supplemental Figure S7A, Supplemental Table S9). *ABCA1* was common to both miR-140-5p and miR-140-3p.1. Furthermore, *ABCA1* was inversely correlated with *WWP2* across multiple skeletal datasets, with the inverse correlation being strongest in cartilage experiments (Supplemental Figure S7B), where miR-140 expression is highest.

DISCUSSION

IsomiRs of miR-140-3p have previously been detected in chondrocytes (Haseeb et al. 2017), breast cancer cell lines (Salem et al. 2016) and endometrial tissue (Krawczynski et al. 2015), and are now recognised in TargetScan 7.2 (Agarwal et al. 2015b). In TargetScan and this study, miR-140-3p.2 refers to the miRNA sequences with the seed of the original miRBase annotation and miR-140-3p.1 refers to the miRNA sequences with the seed of the newly identified isomiR. This study focuses upon the impact of seed sequence (5′isomiRs), further investigation is therefore required to understand the role of 3′ isomiRs of miR-140-3p. miRBase does not currently include specific annotation for isomiRs. In addition to miR-140-3p isomiRs, we detected isomiRs for a number of other miRNAs in cartilage, including miR-455, which is also now recognised in TargetScan 7.2 (Agarwal et al. 2015b). Sequence analysis of the miR-1246 isomiR, suggests it may in fact be miR-1290. According to miRBase these two miRNAs are transcribed from two separate loci on chromosome 2 and 1, respectively. However, Mazieres *et al.* (Mazieres et al. 2013), suggest miR-1246 and miR-1290 are processed from a common transcript (*RNU2*), which explains their similar sequence and expression pattern during chondrogenesis (Barter et al. 2015). Many of the other detected cartilage isomiRs can be transcribed from more than one genomic location (hsa-mir-199a-3p, hsa-mir-199b-3p, hsa-mir-29b, hsa-mir-101, hsa-mir-320c, hsa-mir-103b), raising the possibility that each genomic location gives rise to only one mature miRNA, which are then perceived as isomiRs.

Primary miRNA transcripts are processed to pre-miRNAs in the nucleus by DROSHA (a dsRNA nuclear type III endoribonuclease) facilitated by DGCR8, and subsequently cleaved in the cytoplasm by DICER to generate functionally mature miRNAs molecules. IsomiRs are generated because both DICER and DROSHA process miRNA precursors imprecisely generating miRNA variants with several plus/minus nucleotides at the 5′ and/or 3′ (Neilsen et al. 2012). In addition, miRNAs can also be post-transcriptionally adenylated or uridylated, which could modify miRNA targeting properties and/or their stability (Burroughs et al. 2010; Marzi et al. 2016). The importance of endogenously expressed 5′ isomiRs has been demonstrated by Chiang *et al*. (Chiang et al. 2010), where they showed deletion of miR-223 in mouse neutrophils (Baek et al. 2008), resulted in an increase in expression of predicted targets of a lesser expressed 5′ isomiR of the microRNA. Although it is established 5′ isomiRs can regulate gene expression, the functional reason for their presence is still debated. 5′isomiRs of a given microRNA can have highly over-lapping targets, potentially increasing the specificity of regulation of a particular pathways (Cloonan et al. 2011; Llorens et al. 2013). However, 5′ isomiRs can also increase a microRNAs target repertoire (Tan et al. 2014). Manzano *et al.*, suggest these apparent discrepancies are dependent upon the presence or absence of a U at position 2 of the longer isomiR sequence (Manzano et al. 2015). miR-140-3p.2, the longest 5′ isomiR of miR-140-3p, does not possess a U at position 2, which would suggest miR-140-3p.1 and miR-140-3p.2 have divergent target repertoires,

decreasing their effect on any single target (Manzano et al. 2015). Although not directly studied here, 3′isomiRs are widespread, with 3′ adenine additions being most common and reported to decrease the targeting ability of the miRNA (Burroughs et al. 2010). Some of the miR-140-3p isomiRs with the same seeds as miR-140-3p.1 and miR-140-3p.2 have 3′ adenine additions, which in combination with divergent 5′isomiRs may account for the poor target repression by miR-140-3p.1 and miR-140-3p.2 compared with miR-140-5p. Interestingly, there is an inverse correlation between the ability to repress targets (miR-140-5p>miR-140-3p.1>miR-140-3p.2) and expression in cartilage (miR-140-3p.2>miR-140-3p.2>miR-140-5p).

A mutation within miR-140-5p has recently been identified as causing a human skeletal dysplasia (Grigelioniene et al. 2019b). Mice with the corresponding miR-140-5p mutation phenocopy the human situation and display a loss of miR-140-5p target repression (in rib chondrocytes). This is thought to contribute to the phenotype since the expression of miR-140-3p.1 and miR-140-3.2 were not affected by the mutation. Interestingly though, the phenotypes of the miR-140-5p mutant mice and *MIR140* null mice show some differences, which could perhaps be accounted for by the latter animals lacking miR-140-3p and the isomiRs described here.

Here we identify discrete targets for miR-140-3p.1 and miR-140-3p.2. LIPA, a cholesterol ester hydrolase, is a target of miR-140-3p.1 but not miR-140-3p.2. *LIPA* expression decreases during chondrocyte development in human (Wu et al. 2013), consistent with high miR-140-3p.1 expression in chondrocytes. SDC4 (Syndecan-4), a target of miR-140-3p.2 but not miR-140-3p.1, has been implicated in osteoarthritis progression through activation of ADAMTS5 (Echtermeyer et al. 2009), suggesting *SDC4* suppression by miR-140-3p.2 may maintain a healthy cartilage phenotype. *HMGCR* and *HMGCS1* have now been identified as targets of miR-140-3p.1 in breast cancer cells (Bhardwaj and Cancer … 2018), however their expression was not repressed by miR-140-3p.1 in human chondrocytes, indicating miR-140 isomiRs act in a tissue-specific manner. Even where repression was determined, the effects of miR-140-3p.1 and miR-140-3p.2 were relatively small (up to ~25% repression) when compared to the effects of miR-140-5p on a previously published miR-140-5p direct target, FZD6 (~60% repression) (Barter et al. 2015). Furthermore, contra to the expected miR-140-3p.1 repression of targets, miR-140-3p.1 increased luciferase for the *MARCKSL1*, *KIAA1199* and *MAPILC3A* 3′UTR constructs, possibly suggesting stabilisation of transcript, as previously described for miR-322 and *MEK1* (Bluhm et al. 2017).

The target repertoire of miR-140-3p.1 and miR-140-3p.2 are vastly different, due to established miRNA target interaction rules. The only shared binding motif is ‘CUGUGG’, which can be recognised by miR-140-3p.1 as a 6merBS (CUGUGG), or by miR-140-3p.2 as a 7m8-BS or 8mer-BS if followed by U or UA, respectively (CUGUGG**U** or CUGUGG**UA**) (Figure 2A). Indeed the miR-140-3p.1 6merBS (CUGUGG) was the most enriched miR-140-3p.1

motif following miR-140-3p.2 transfection (Figure 3E; red line in bottom right), indicating miR-140-3p isomiRs act according to traditional miRNA targeting rules. Other types of miRNA binding sites such as 3′compensatory binding (Grimson et al. 2007) may be shared between miR-140-3p.1 and miR-140-3p.2, but are less common and more difficult to predict.

Analysis of miRNA target interactions within published skeletal data sets, using the *WWP2* host gene as a surrogate for miRNA expression, along with directly overexpressing the miRNAs and observing changes in gene expression, suggests these types of analyses can improve miRNA target prediction within skeletal tissues. Caution must however be taken as *WWP2* and miR-140 can display tissue specific expression (Yamashita et al. 2012), furthermore, miRNA are often co-expressed with their targets as part of a larger more complex network (Cora et al. 2017). This type of co-expression may account for the studies where a correlation, rather than an inverse correlation, between *WWP2* and miR-140 targets was observed. Where an inverse correlation was observed between *WWP2* and miR-140 predicted targets this was greatest within cartilage. Together, these data indicate the miR-140-3p isomiR miR-140-3p.1 can function to down-regulate transcript expression *in vitro* and *in vivo*.

In conclusion, analysis of human cartilage sRNA-seq identified an abundant isomiR to miR-140-3p, miR-140-3p.1. Functional analysis in human and murine chondrocytes and analysis of published skeletal datasets suggests the newly identified isomiR is more effective than the original miR-140-3p annotated in miRBase. These data suggest the function of miR-140-3p, which has previously been largely ignored, should be revisited.

ACCESSION NUMBERS

Microarray data and RNA-seq data are available at NCBI GEO datasets with the accession numbers GSE144374.

SUPPLEMENTARY DATA

Supplementary Data are available online.

ACKNOWLEDGEMENT

pLKO.1-puro U6 sgRNA BfuAI large stuffer was a gift from Scot Wolfe (Addgene plasmid # 52628 ; http://n2t.net/addgene:52628 ; RRID:Addgene_52628).

FUNDING

This work was supported by the Oliver Bird Rheumatism Programme (Nuffield Foundation); Medical Research Council and Versus Arthritis as part of the MRC-Arthritis Research UK

Centre for Integrated Research into Musculoskeletal Ageing (CIMA) [JXR 10641, MR/P020941/1]; Versus Arthritis [19424, 22043]; the JGW Patterson Foundation; The Dunhill Medical Trust [R476/0516); and the NIHR Newcastle Biomedical Research.

CONFLICT OF INTEREST

All authors declare no conflicts of interest.

REFERENCES

Agarwal V, Bell GW, Nam JW, Bartel DP. 2015a. Predicting effective microRNA target sites in mammalian mRNAs. *Elife* **4**.

-. 2015b. Predicting effective microRNA target sites in mammalian mRNAs. *elife* **4**: e05005.

Baek D, Villen J, Shin C, Camargo FD, Gygi SP, Bartel DP. 2008. The impact of microRNAs on protein output. *Nature* **455**: 64-71.

Bartel DP. 2004. MicroRNAs: genomics, biogenesis, mechanism, and function. *Cell* **116**: 281-297.

-. 2009. MicroRNAs: target recognition and regulatory functions. *Cell* **136**: 215-233.

Barter MJ, Tselepi M, Gómez R, Woods S, Hui W, Smith GR, Shanley DP, Clark IM, Young DA. 2015. Genome-Wide MicroRNA and Gene Analysis of Mesenchymal Stem Cell Chondrogenesis Identifies an Essential Role and Multiple Targets for miR-140-5p. *Stem cells (Dayton, Ohio)* **33**: 3266-3280.

Bhardwaj A, Cancer … S-H. 2018. The isomiR-140-3p-regulated mevalonic acid pathway as a potential target for prevention of triple negative breast cancer. *Breast Cancer …*.

Bluhm B, Ehlen HWA, Holzer T, Georgieva VS, Heilig J, Pitzler L, Etich J, Bortecen T, Frie C, Probst K et al. 2017. miR-322 stabilizes MEK1 expression to inhibit RAF/MEK/ERK pathway activation in cartilage. *Development* **144**: 3562-3577.

Burroughs AM, Ando Y, de Hoon MJ, Tomaru Y, Nishibu T, Ukekawa R, Funakoshi T, Kurokawa T, Suzuki H, Hayashizaki Y et al. 2010. A comprehensive survey of 3' animal miRNA modification events and a possible role for 3' adenylation in modulating miRNA targeting effectiveness. *Genome research* **20**: 1398-1410.

Burroughs AM, Ando Y, de Hoon MJ, Tomaru Y, Suzuki H, Hayashizaki Y, Daub CO. 2011. Deep-sequencing of human Argonaute-associated small RNAs provides insight into miRNA sorting and reveals Argonaute association with RNA fragments of diverse origin. *RNA Biol* **8**: 158-177.

Chiang HR, Schoenfeld LW, Ruby JG, Auyeung VC, Spies N, Baek D, Johnston WK, Russ C, Luo S, Babiarz JE et al. 2010. Mammalian microRNAs: experimental evaluation of novel and previously annotated genes. *Gene Dev* **24**: 992-1009.

Cloonan N, Wani S, Xu Q, Gu J, Lea K, Heater S, Barbacioru C, Steptoe AL, Martin HC, Nourbakhsh E et al. 2011. MicroRNAs and their isomiRs function cooperatively to target common biological pathways. *Genome biology* **12**: R126.

Cora D, Re A, Caselle M, Bussolino F. 2017. MicroRNA-mediated regulatory circuits: outlook and perspectives. *Phys Biol* **14**.

Crowe N, Swingler TE, Le LT, Barter MJ, Wheeler G, Pais H, Donell ST, Young DA, Dalmay T, Clark IM. 2016. Detecting new microRNAs in human osteoarthritic chondrocytes identifies miR-3085 as a human, chondrocyte-selective, microRNA. *Osteoarthritis and cartilage* **24**: 534-543.

Echtermeyer F, Bertrand J, Dreier R, Meinecke I, Neugebauer K, Fuerst M, Lee YJ, Song YW, Herzog C, Theilmeier G et al. 2009. Syndecan-4 regulates ADAMTS-5 activation and cartilage breakdown in osteoarthritis. *Nat Med* **15**: 1072-1076.

Flores O, Kennedy EM, Skalsky RL, Cullen BR. 2014. Differential RISC association of endogenous human microRNAs predicts their inhibitory potential. *Nucleic acids research* **42**: 4629-4639.

Franca GS, Vibranovski MD, Galante PA. 2016. Host gene constraints and genomic context impact the expression and evolution of human microRNAs. *Nat Commun* **7**: 11438.

Gennarino VA, Sardiello M, Avellino R, Meola N, Maselli V, Anand S, Cutillo L, Ballabio A, Banfi S. 2009. MicroRNA target prediction by expression analysis of host genes. *Genome research* **19**: 481-490.

Griffiths-Jones S. 2004. The microRNA Registry. *Nucleic acids research* **32**: D109-111.

Grigelioniene G, Suzuki HI, Taylan F, Mirzamohammadi F, Borochowitz ZU, Ayturk UM, Tzur S, Horemuzova E, Lindstrand A, Weis MA et al. 2019a. Gain-of-function mutation of microRNA-140 in human skeletal dysplasia. *Nat Med*.

-. 2019b. Gain-of-function mutation of microRNA-140 in human skeletal dysplasia. *Nat Med* **25**: 583-590.

Grimson A, Farh KK, Johnston WK, Garrett-Engele P, Lim LP, Bartel DP. 2007. MicroRNA targeting specificity in mammals: determinants beyond seed pairing. *Molecular cell* **27**: 91-105.

Haseeb A, Makki MS, Khan NM, Ahmad I, Haqqi TM. 2017. Deep sequencing and analyses of miRNAs, isomiRs and miRNA induced silencing complex (miRISC)-associated miRNome in primary human chondrocytes. *Scientific reports* **7**: 15178.

Huang da W, Sherman BT, Lempicki RA. 2009. Systematic and integrative analysis of large gene lists using DAVID bioinformatics resources. *Nat Protoc* **4**: 44-57.

Ittner LM, Gotz J. 2007. Pronuclear injection for the production of transgenic mice. *Nat Protoc* **2**: 1206-1215.

Kozomara A, Griffiths-Jones S. 2011. miRBase: integrating microRNA annotation and deep-sequencing data. *Nucleic acids research* **39**: D152-157.

Krawczynski K, Bauersachs S, Reliszko ZP, Graf A, Kaczmarek MM. 2015. Expression of microRNAs and isomiRs in the porcine endometrium: implications for gene regulation at the maternal-conceptus interface. *BMC Genomics* **16**: 906.

Kuchen S, Resch W, Yamane A, Kuo N, Li Z, Chakraborty T, Wei L, Laurence A, Yasuda T, Peng S et al. 2010. Regulation of microRNA expression and abundance during lymphopoiesis. *Immunity* **32**: 828-839.

Lewis BP, Burge CB, Bartel DP. 2005. Conserved seed pairing, often flanked by adenosines, indicates that thousands of human genes are microRNA targets. *Cell* **120**: 15-20.

Llorens F, Bañez-Coronel M, Pantano L. 2013. A highly expressed miR-101 isomiR is a functional silencing small RNA. *BMC …*.

Love MI, Huber W, Anders S. 2014. Moderated estimation of fold change and dispersion for RNA-seq data with DESeq2. *Genome biology* **15**: 550.

Manzano M, Forte E, Raja AN, Schipma MJ, Gottwein E. 2015. Divergent target recognition by coexpressed 5'-isomiRs of miR-142-3p and selective viral mimicry. *Rna* **21**: 1606-1620.

Marzi MJ, Ghini F, Cerruti B, de Pretis S, Bonetti P, Giacomelli C, Gorski MM, Kress T, Pelizzola M, Muller H et al. 2016. Degradation dynamics of microRNAs revealed by a novel pulse-chase approach. *Genome research* **26**: 554-565.

Mazieres J, Catherinne C, Delfour O, Gouin S, Rouquette I, Delisle MB, Prevot G, Escamilla R, Didier A, Persing DH et al. 2013. Alternative processing of the U2 small nuclear RNA produces a 19-22nt fragment with relevance for the detection of non-small cell lung cancer in human serum. *PLoS ONE* **8**: e60134.

Metsalu T, Vilo J. 2015. ClustVis: a web tool for visualizing clustering of multivariate data using Principal Component Analysis and heatmap. *Nucleic acids research* **43**: W566-570.

Miyaki S, Nakasa T, Otsuki S, Grogan SP, Higashiyama R, Inoue A, Kato Y, Sato T, Lotz MK, Asahara H. 2009. MicroRNA-140 is expressed in differentiated human articular chondrocytes and modulates interleukin-1 responses. *Arthritis and rheumatism* **60**: 2723-2730.

Miyaki S, Sato T, Inoue A, Otsuki S, Ito Y, Yokoyama S, Kato Y, Takemoto F, Nakasa T, Yamashita S et al. 2010. MicroRNA-140 plays dual roles in both cartilage development and homeostasis. *Gene Dev* **24**: 1173-1185.

Moore MJ, Scheel TK, Luna JM, Park CY, Fak JJ, Nishiuchi E, Rice CM, Darnell RB. 2015. miRNA-target chimeras reveal miRNA 3'-end pairing as a major determinant of Argonaute target specificity. *Nat Commun* **6**: 8864.

Morin RD, O'Connor MD, Griffith M, Kuchenbauer F, Delaney A, Prabhu AL, Zhao Y, McDonald H, Zeng T, Hirst M et al. 2008. Application of massively parallel sequencing to microRNA profiling and discovery in human embryonic stem cells. *Genome research* **18**: 610-621.

Neilsen CT, Goodall GJ, Bracken CP. 2012. IsomiRs--the overlooked repertoire in the dynamic microRNAome. *Trends Genet* **28**: 544-549.

Patro R, Duggal G, Love MI, Irizarry RA, Kingsford C. 2017. Salmon provides fast and bias-aware quantification of transcript expression. *Nature methods* **14**: 417-419.

Radfar MH, Wong W, Morris Q. 2011. Computational prediction of intronic microRNA targets using host gene expression reveals novel regulatory mechanisms. *PLoS One* **6**: e19312.

Ran FA, Hsu PD, Wright J, Agarwala V, Scott DA, Zhang F. 2013. Genome engineering using the CRISPR-Cas9 system. *Nat Protoc* **8**: 2281-2308.

Raudvere U, Kolberg L, Kuzmin I, Arak T, Adler P, Peterson H, Vilo J. 2019. g:Profiler: a web server for functional enrichment analysis and conversions of gene lists (2019 update). *Nucleic acids research* **47**: W191-W198.

Risso D, Ngai J, Speed TP, Dudoit S. 2014. Normalization of RNA-seq data using factor analysis of control genes or samples. *Nat Biotechnol* **32**: 896-902.

Salem O, Erdem N, Jung J, Munstermann E, Worner A, Wilhelm H, Wiemann S, Korner C. 2016. The highly expressed 5'isomiR of hsa-miR-140-3p contributes to the tumor-suppressive effects of miR-140 by reducing breast cancer proliferation and migration. *BMC Genomics* **17**: 566.

Shah A, Qian Y, Weyn-Vanhentenryck SM, Zhang C. 2017. CLIP Tool Kit (CTK): a flexible and robust pipeline to analyze CLIP sequencing data. *Bioinformatics* **33**: 566-567.

Smyth GK. 2004. Linear models and empirical bayes methods for assessing differential expression in microarray experiments. *Statistical applications in genetics and molecular biology* **3**: Article3.

Sorefan K, Pais H, Hall AE, Kozomara A, Griffiths-Jones S, Moulton V, Dalmay T. 2012. Reducing ligation bias of small RNAs in libraries for next generation sequencing. *Silence* **3**: 4.

Soul J, Hardingham T, Boot-Handford R, Schwartz JM. 2018. SkeletalVis: An exploration and meta-analysis data portal of cross-species skeletal transcriptomics data. *Bioinformatics*.

Stark MS, Tyagi S, Nancarrow DJ, Boyle GM, Cook AL, Whiteman DC, Parsons PG, Schmidt C, Sturm RA, Hayward NK. 2010. Characterization of the Melanoma miRNAome by Deep Sequencing. *PLoS ONE* **5**: e9685.

Tan G, Chan E, Molnar A, Sarkar R, Alexieva D, Isa I, Robinson S, Zhang S, Ellis P, Langford CF. 2014. 5 isomiR variation is of functional and evolutionary importance. *Nucleic acids research* **42**: 9424-9435.

van Dongen S, Abreu-Goodger C, Enright AJ. 2008. Detecting microRNA binding and siRNA off-target effects from expression data. *Nature methods* **5**: 1023-1025.

Wienholds E, Kloosterman WP, Miska E, Alvarez-Saavedra E, Berezikov E, de Bruijn E, Horvitz HR, Kauppinen S, Plasterk RH. 2005. MicroRNA expression in zebrafish embryonic development. *Science* **309**: 310-311.

Witten D, Tibshirani R, Gu SG, Fire A, Lui WO. 2010. Ultra-high throughput sequencing-based small RNA discovery and discrete statistical biomarker analysis in a collection of cervical tumours and matched controls. *Bmc Biol* **8**.

Woods S, Barter MJ, Elliott HR, McGillivray CM, Birch MA, Clark IM, Young DA. 2019. miR-324-5p is up regulated in end-stage osteoarthritis and regulates Indian Hedgehog signalling by differing mechanisms in human and mouse. *Matrix Biol* **77**: 87-100.

Wu L, Bluguermann C, Kyupelyan L, Latour B, Gonzalez S, Shah S, Galic Z, Ge SD, Zhu YH, Petrigliano FA et al. 2013. Human Developmental Chondrogenesis as a Basis for Engineering Chondrocytes from Pluripotent Stem Cells. *Stem Cell Rep* **1**: 575-589.

Wyman SK, Knouf EC, Parkin RK, Fritz BR, Lin DW, Dennis LM, Krouse MA, Webster PJ, Tewari M. 2011. Post-transcriptional generation of miRNA variants by multiple nucleotidyl transferases contributes to miRNA transcriptome complexity. *Genome research* **21**: 1450-1461.

Yamashita S, Miyaki S, Kato Y, Yokoyama S, Sato T, Barrionuevo F, Akiyama H, Scherer G, Takada S, Asahara H. 2012. L-Sox5 and Sox6 proteins enhance chondrogenic miR-140 microRNA expression by strengthening dimeric Sox9 activity. *The Journal of biological chemistry* **287**: 22206-22215.

Yang H, Wang H, Shivalila CS, Cheng AW, Shi L, Jaenisch R. 2013. One-step generation of mice carrying reporter and conditional alleles by CRISPR/Cas-mediated genome engineering. *Cell* **154**: 1370-1379.

MAIN FIGURE LEGENDS

Figure 1. miR-140-3p isomiRs are abundantly expressed in cartilage. (A) Pie chart illustrating the relative abundance of all miRNAs expressed in cartilage, data combines isomiR and canonical reads for each miRNA. (B) Pie chart illustrating the isomiR type for all reads aligned to miR-140-3p. (C) Pie chart illustrating seed sequences for all reads aligned to miR-140-3p, >99% of reads have one of two seed sequences; ACCACAG (blue) and CCACAGG (red). (D) Pie chart of the percentage of templated and non-templated reads for miR-140-3p within cartilage. (E) Histogram of all sequencing reads aligned to miR-140-3p in cartilage. (F) Histogram of sequencing reads aligned to miR-140-3p, whose 5' end is as indicated in miRBase. (G) Histogram of sequencing reads aligned to miR-140-3p, whose 5' end is one nucleotide shorter than indicated in miRBase. (H) Bar chart indicting the sequences and number of reads that contribute to each of the two seed sequences. Individual bars represent total read number from 3 separate individuals. (I) qRT-PCR for miR-140-3p.1 and miR-140-3p.2. Assays designed to detect each isomiR are able to distinguish between miR-140-3p.1 and miR-140-3p.2 spike-ins (2-fold serial dilution) and detect high expression of each isomiR in cartilage (2-fold serial dilution).

Figure 2. miR-140-3p.1 and miR-140-3p.2 are predicted to have distinct targets. (A) Schematic illustrating the sequences of miRBase miR-140-3p, miR-140-3p.1, miR-140-3p.2 and miR-140-5p and their potential binding sites within target mRNAs using the TargetScan categorisation. (B) Venn diagram illustrating little cross over of targets predicted by TargetScan 7.2 for miR-140-3p.1, miR-140-3p.2 and miR-140-5p.

Figure 3. Identification and validation of miR-140-3p.1 and miR-140-3p.2 targets in human chondrocytes. (A) qRT-PCR for miR-140-3p.1 and miR-140-3p.2 following transfection of either control mimic, miR-140-3p.1 mimic or miR-140-3p.2 mimic for 48h. (B) PCA of whole genome micro-array following transfection of mimics described in (A), (140.1= miR-140-3p.1 and 140.2=miR-140-3p.2). (C) Heat map of whole genome micro-array following transfection of mimics as described in (A) (140.1= miR-140-3p.1 and 140.2=miR-140-3p.2). (D) Venn diagram indicating the number of genes downregulated following overexpression of miR-140-3p.1 and miR-140-3p.2. (E) Enrichment analysis using Sylamer for 3'UTR mRNA motifs complementary to either miR-140-3p.1 or miR-140-3p.2 seed sequences in genes whose expression decreased following transfection of either miR-140-3p mimic, miR-140-3p.1 mimic or miR-140-3p.2 mimic. (F) Gene expression changes of miR-140-3p.1 (only.1; red triangles), miR-140-3p.2 (only.2; blue diamonds) or miR-140-3p.1 and miR-140-3p.2 (common; black squares) predicted targets following transfection of either miR-140-3p.1 mimic or miR-140-3p.2 mimic. (G-I) 3'UTR luciferase reporters for miR-140-3p.1 and miR-140-3p.2 putative targets. *, ** or *** indicate level of significance ($p<0.05$, 0.01 or 0.001, respectively) of either miR-140-3p.1 or miR-140-3p.2 to control. # indicates level of significance ($p<0.05$, 0.01 or 0.001, respectively) between miR-140-3p.1 and miR-140-3p.2.

Figure 4. Evidence for functional miR-140-3p.1 and miR-140-3p.2 in mouse cartilage. (A) Pie chart illustrating the fraction of miR-140-3p reads with canonical 5′ and 3′ ends (grey), canonical 5′ and either shorter or longer 3′ (blue), canonical 3′ and either shorter or longer 5′ (green), either shorter or longer 5′ and either shorter or longer 3′ (red). (B) As in (A) with miR-140-3p.1 and miR-140-3p.2 indicated in dark red and dark blue respectively. (C) Bar chart indicting number of reads that contribute to (B). (D) % of genes that are predicted targets of either a miR-140-5p (green), miR-140-3p.1 (red) or miR-140-3p.2 (blue), in genes whose expression decrease, does not change or increase following KO of miR-140 in mice. (E) Median fold change (FC) of all genes that are predicted targets of either a miR-140-5p (green), miR-140-3p.1 (red) or miR-140-3p.2 (blue) following KO of miR-140 in mice. (F) Cumulative fraction plot of all genes (black), miR-140-5p (green), miR-140-3p.1 (red) or miR-140-3p.2 (blue) predicted targets, for genes ordered from most decreased expression to most increased expression in *Mir140* null mice. Inset: Fraction at a cut-off of log2FC -1. (G) Sylamer analysis for *Mir140* null mice; the 100 most enriched 7mers are shown with 7m8 binding sites for miR-140-5p (green), miR-140-3p.1 (red) and miR-140-3p.2 (blue) highlighted.

Figure 5. Evidence for miR-140-3p.1 and miR-140-3p.2 function during human MSC chondrogenesis. Re-analysis of data from Barter *et al* [10] for human MSC differentiation to cartilage. (A) Changes in gene expression for eight MSC and chondrogenic markers. (B) Mean fold change of all genes that are predicted targets of either a miR-140-5p (green), miR-140-3p.1 (red) or miR-140-3p.2 (blue) during MSC chondrogenesis. (C) Sylamer analysis for a miR-140-5p (green), miR-140-3p.1 (red) and miR-140-3p.2 (blue) 7m8 seed sequences.

Figure 6. Correlation of *MIR140* locus host gene *WWP2* with miR-140 target genes in SkeletalVis transcriptomic datasets. (A-D) Correlation analysis of *WWP2* and predicted miRNA target expression in 124 pre-existing transcriptome-wide comparisons (both human and mouse). Scatter graph of *WWP2* log2FC plotted against the average log2FC for genes predicted to be either a target of miR-140-5p (A), miR-140-3p.1 (B), miR-140-3p.2 (C) or 500 random genes (D), p-value calculated from linear regression analysis. (E-H) Percentage of miR-140-5p (E), miR-140-3p.1 (F) or miR-140-3p.2 (G) predicted targets and 500 random genes (H) within the significantly up or downregulated genes for data sets where *WWP2* expression significantly changes. The percentage of targets within upregulated (purple), no change (black) or downregulated (orange) transcripts is plotted against log2FC *WWP2*. Large icons represent enrichment of miR-140-5p, miR-140-3p.1 and miR-140-3p.2 predicted targets in up- and downregulated genes within rib cartilage of *Mir140* null mice, where *Wwp2* expression does not change.

SUPPLEMENTAL FIGURE LEGENDS

Supplemental Figure S1. Cartilage miRNAs which have abundant 5′ isomiRs. Twenty-nine miRNAs with isomiRs that account for more than 5% of the reads for that miRNA and the number of isomiR reads is greater than 100. miR-1246 isomiR (read count 99) is also shown. 5′ start position of each isomiR relative to the miRBase annotation is shown: the addition of a nucleotide is designated as '+1' and the loss as '-1', '0' represents reads of the miRBase annotation. Histogram indicates read count.

Supplemental Figure S2. Analysis of published RNA-seq. miR-140-3p.1 and miR-140-3p.2 were present in multiple sRNA-seq data including; melanoma (Stark et al. 2010), cervix (Witten et al. 2010), lymphocytes (Kuchen et al. 2010), and following immunoprecipitation of Argonaute (AGO) proteins (Burroughs et al. 2011). Sequences were designated either miR-140-3p.1 or miR-140-3p.2 based upon seed sequence. The isomiRs were also approximately equally detected in CLEAR-CLIP data from mouse cortex tissue (Moore et al. 2015), however their low expression in this tissue did not allow for target prediction from the covalently ligated mRNAs.

Supplemental Figure S3. Pathway analysis of differentially expressed genes using g-Profiler. Pathway analysis of the 237 genes differentially expressed between miR-140-3p.1 and miR-140-3p.2 transfected chondrocytes using g-Profiler. Significant gene ontology molecular function (G0:MF), biological processes (GO:BP) and Reactome (REAC) terms are shown. The adjusted p-values, distribution within terms between downregulation with each isomiR and the fraction of these genes that are also predicted targets of miR-140-3p.1 and miR-140-3p.2 are depicted. Distribution of miR-140-3p.1 and miR-140-3p.2 TargetScan predicted targets (PT) are also shown.

Supplemental Figure S4. IsomiR read count and enrichment score for all possible sequences derived from miR-140. (A) Read count for all 5′isomiRs encoded from the mouse miR-140 stem loop according to miRBase. (B) Sylamer analysis of rib cartilage RNA from mice lacking miR-140 stem loop for 7m8 seed binding sites corresponding to every possible miRNA produced from the *Mir140* locus. Histogram represents average enrichment score for each seed binding motif.

Supplemental Figure S5. Validation of miR-140 null mouse model and rib chondrocyte RNA-seq. (A) Deletion of *Mir140* was attained using the CRISPR/-Cas9 system. The *Mir140* locus was targeted in mouse zygotes using two crRNAs (blue line, protospacer adjacent motif (PAM) shown in red). This successfully deleted the *Mir140* locus sequence depicted (KO mir140). (B) Mice were bred to homozygosity with the genotype in wild-type, heterozygous and null mice confirmed through PCR of ear-notch genomic RNA. (C) Total RNA was extracted from rib chondrocytes of postnatal day 7 (P7) mice, reverse transcribed to cDNA and subjected to real time qRT-PCR analysis for gene expression of miR-140-5p and miR-

140-3p (canonical). Values were normalised to U6 and plotted as mean ± standard error of the mean (SEM) (number of samples, WT=7, miR-140$^{-/-}$ =6). *** p≤0.001. (D) The RNA from several of the same samples as (C) was subjected to RNA-seq (n=4 for WT and miR-140$^{-/-}$). Principle component analysis of length-scaled TPM (Transcripts Per Million) values segregated WT and KO (blue and red). (E) Heat map of the 1200 most differentially expressed genes.

Supplemental Figure S6. Comparison of miR-140-5p, miR-140-3p.1 and miR-140-3p.2 target fold change and enrichment in studies where *WWP2* expression either decrease or increases. (A) Average log2FC for miR-140-5p, miR-140-3p.1 and miR-140-3p.2 targets within studies where *WWP2* expression either decreased for increased. (B) Correlation between average log2FC for miR-140-5p, miR-140-3p.1 and miR-140-3p.2 predicted targets for all studies where *WWP2* expression changed. (C) Enrichment for miR-140-5p, miR-140-3p.1 and miR-140-3p.2 targets within studies where *WWP2* either decreased for increased. (D) Correlation between enrichment for miR-140-5p, miR-140-3p.1 and miR-140-3p.2 predicted targets for all studies where *WWP2* expression changed. Studies where *WWP2* significantly decreased are shown in purple and increased shown in orange. For (B) and (C) symbol size if proportional to the level of *WWP2* change in expression. The enrichment was calculated by dividing the percentage of targets within upregulated genes by the percentage of targets within downregulated genes for each study.

Supplemental Figure S7. Overlap between human and mouse miR140 datasets. (A) overlap between predicted targets, genes downregulated following overexpression in human articular chondrocytes (HAC), genes upregulated in mice lacking the *Mir140* locus and genes downregulated during human MSC chondrogenesis. Data represented as Venn diagram and 'UpSet' plot. (B) Regression analysis of *ABCA1* expression and *WWP2* in multiple skeletal tissues, separated based on tissue type.

SUPPLEMENTAL TABLE LEGENDS

Supplemental Table S1. Cartilage sRNA-seq. Cartilage sRNA-seq from 3 donors (c15, c16 and c17). All sequences including isomiRs aligning to 990 mature miRNAs are shown with read count.

Supplemental Table S2. Predicted targets. Predicted targets of miR-140-5p, miR-140-3p.1 and miR-140-3p.2 by TargetScanHuman 7.2. Gene lists correspond to Venn diagram in figure 2B.

Supplemental Table S3. Human chondrocyte gene expression. Human chondrocyte gene expression changes following transfection of miRNA mimics: miR-140-3p.1 vs CON, miR-140-3p.2 vs CON, miR-140-3p.1 vs miR-140-3p.2

Supplemental Table S4. Human chondrocyte gene list. Gene lists from human chondrocytes: Genes decreased (down) with miR-140-3p.1 vs control, Genes decreased (down) with miR-140-3p.2 vs control, Genes decreased (down) with both miR-140-3p.1 and miR-140-3p.2 vs control, and genes significantly different between miR-140-3p.1 and miR-140-3p.2 when directly compared.

Supplemental Table S5. Human chondrocyte pathway analysis. Pathway analysis (PA) using DAVID for genes decreased with miR-140-3p.1, genes decreased with miR-140-3p.2 genes significantly different between miR-140-3p.1 and miR-140-3p.2.

Supplemental Table S6. *Mir140* KO mice gene expression. RNA-seq of mouse rib cartilage of *Mir140* KO mice and WT control mice

Supplemental Table S7. *Mir140* KO mice gene lists. List of up and downregulated genes in *Mir140* KO mice

Supplemental Table S8. *Mir140* KO mice pathway analysis. Pathway analysis using DAVID for genes upregulated in *Mir140* KO mice

Supplemental Table S9. Human vs mouse. Cross over between predicted targets, human chondrocyte data and mouse *Mir140* KO data

Supplemental Table S10. Oligonucleotides. Table of oligonucleotides used in this study. Targets of miR-140-3p.1 and miR-140-3p.2 used for cloning into pMiR-GLO by InFusion. Primers used for the generation and genotyping of miR-140$^{-/-}$ mice.

Figure 1

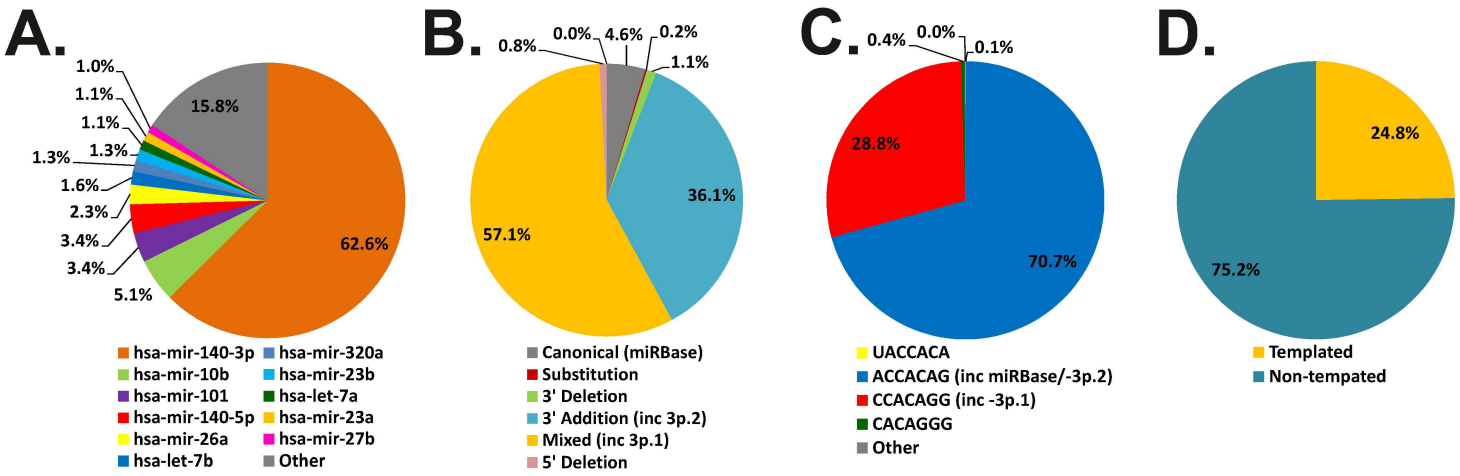
A.
1.0%
1.1%
1.1%
1.3%
1.3%
1.6%
2.3%
3.4%
3.4%
5.1%
15.8%
62.6%
hsa-mir-140-3p
hsa-mir-320a
hsa-mir-10b
hsa-mir-23b
hsa-mir-101
hsa-let-7a
hsa-mir-140-5p
hsa-mir-23a
hsa-mir-26a
hsa-mir-27b
hsa-let-7b
Other
B.
0.8%
0.0%
4.6%
0.2%
1.1%
36.1%
57.1%
Canonical (miRBase)
Substitution
3' Deletion
3' Addition (inc 3p.2)
Mixed (inc 3p.1)
5' Deletion
C.
0.4%
0.0%
0.1%
28.8%
70.7%
UACCACA
ACCACAG (inc miRBase/-3p.2)
CCACAGG (inc -3p.1)
CACAGGG
Other
D.
24.8%
75.2%
Templated
Non-tempated

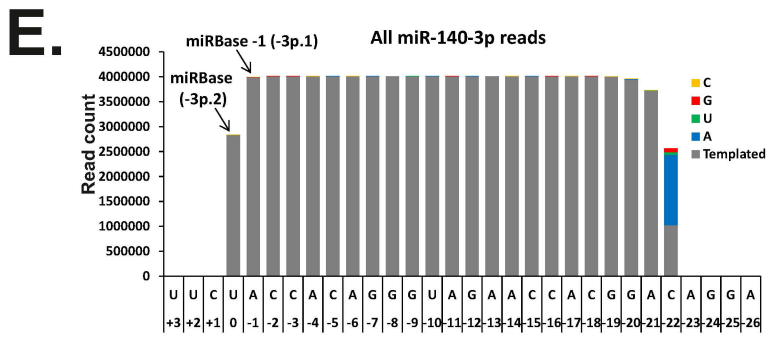
E.
All miR-140-3p reads
miRBase -1 (-3p.1)
miRBase (-3p.2)
Read count
C
G
U
A
Templated

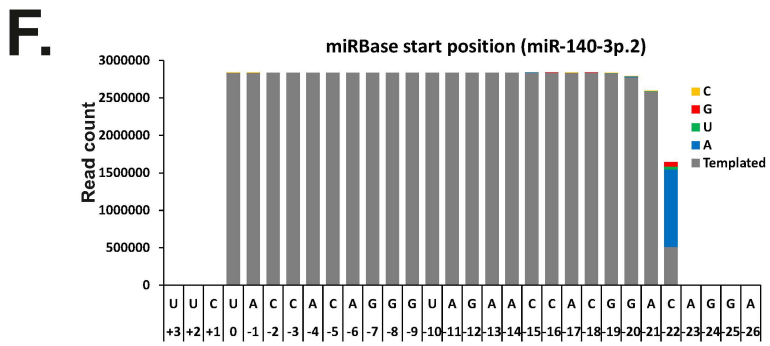
F.
miRBase start position (miR-140-3p.2)
Read count
C
G
U
A
Templated

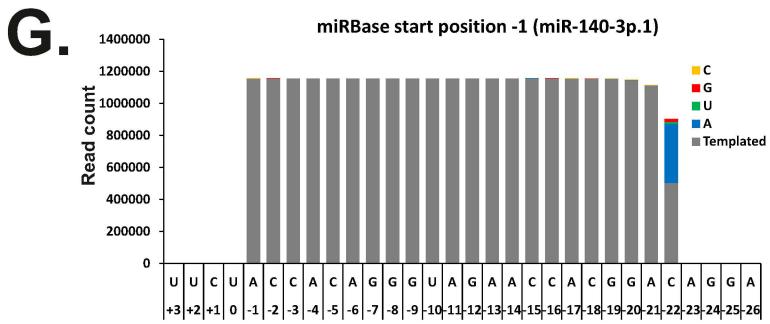
G.
miRBase start position -1 (miR-140-3p.1)
Read count
C
G
U
A
Templated

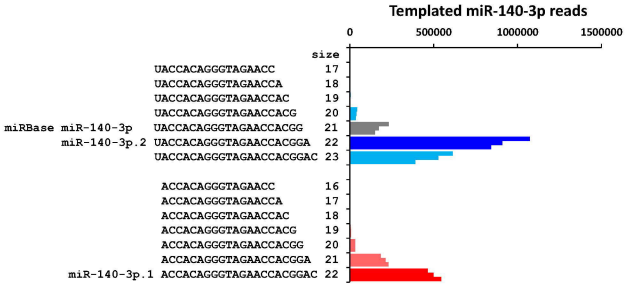
H.
Templated miR-140-3p reads
size
miRBase miR-140-3p
miR-140-3p.2
miR-140-3p.1

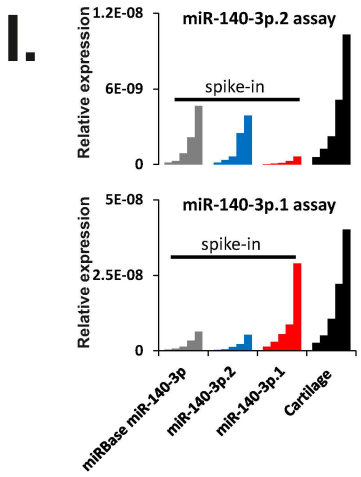
I.
miR-140-3p.2 assay
spike-in
miR-140-3p.1 assay
spike-in
Relative expression
miRBase miR-140-3p
miR-140-3p.2
miR-140-3p.1
Cartilage

A.

```
          miRNA position:12345678                          miRNA postion:87654321
miRBase miR-140-3p 5′ UACCACAGGGUAGAACCACGG 3′     miR-140-3p   8merBS:      CUGUGGUA
                3′ nnnnnUGGUGUCnnnnnnnnnnnnnnnnnnn 5′ miR-140-3p   7mer-m8BS:  CUGUGGU
                                                   miR-140-3p   7mer-1aBS:    UGUGGUA
                                                   miR-140-3p   6merBS:       UGUGGU

          miRNA position:12345678                          miRNA postion:87654321
miR-140-3p.1 5′ _ACCACAGGGUAGAACCACGGAC 3′     miR-140-3p.1 8merBS:      CCUGUGGA
                3′ nnnnnnGGUGUCCnnnnnnnnnnnnnnnnnn 5′ miR-140-3p.1 7mer-m8BS:  CCUGUGG
                                                   miR-140-3p.1 7mer-1aBS:   CUGUGGA
                                                   miR-140-3p.1 6merBS:      CUGUGG

          miRNA position:12345678                          miRNA postion:87654321
miR-140-3p.2  5′ UACCACAGGGUAGAACCACGGA 3′     miR-140-3p.2 8merBS:      CUGUGGUA
                3′ nnnnnUGGUGUCnnnnnnnnnnnnnnnnnnn 5′ miR-140-3p.2 7mer-m8BS:  CUGUGGU
                                                   miR-140-3p.2 7mer-1aBS:    UGUGGUA
                                                   miR-140-3p.2 6merBS:       UGUGGU

          miRNA position:12345678                          miRNA postion:87654321
miR-140-5p  5′  CAGUGGUUUUACCCUAUGGUAG 3′      miR-140-5p   8merBS:      AACCACUA
                3′ nnnnnUCACCAAnnnnnnnnnnnnnnnnnnn 5′ miR-140-5p   7mer-m8BS:  AACCACU
                                                   miR-140-5p   7mer-1aBS:    ACCACUA
                                                   miR-140-5p   6merBS:       ACCACU
```

B.

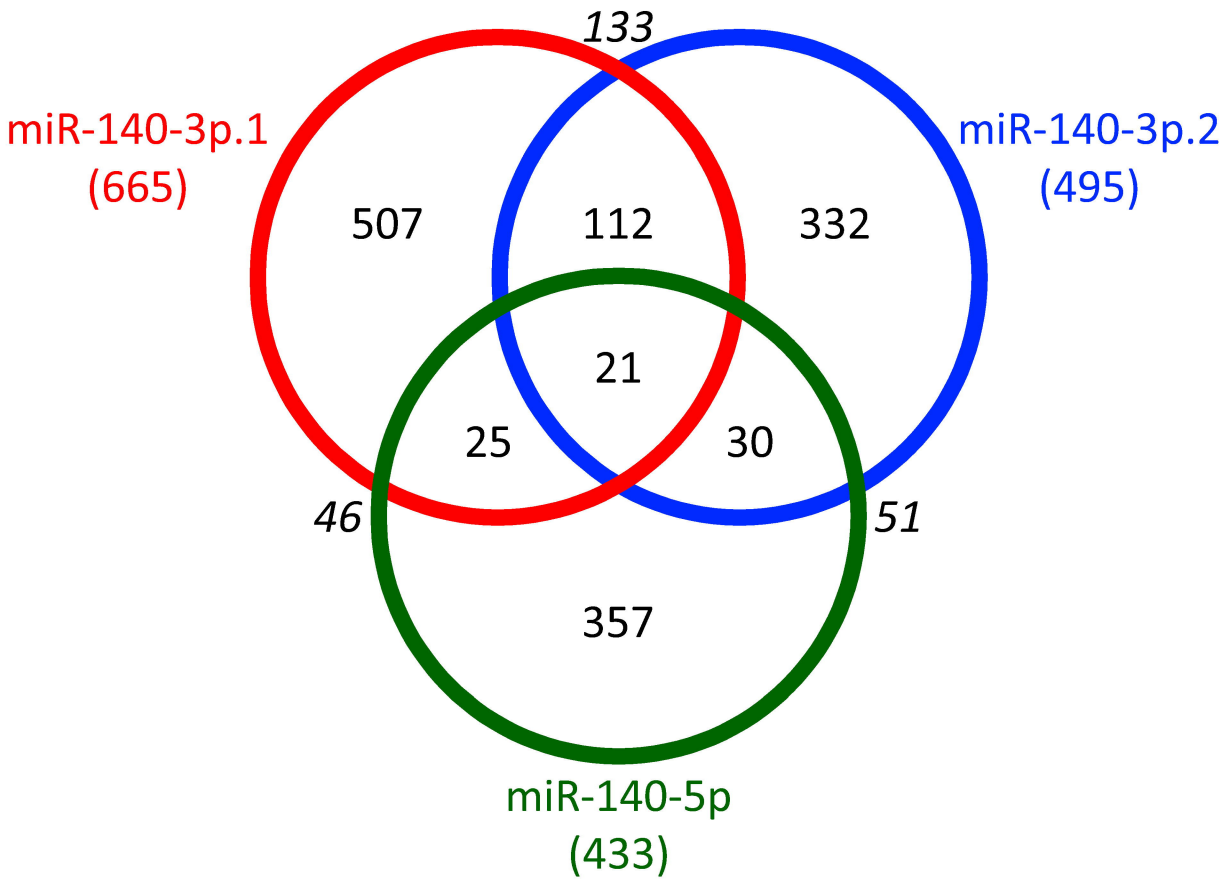

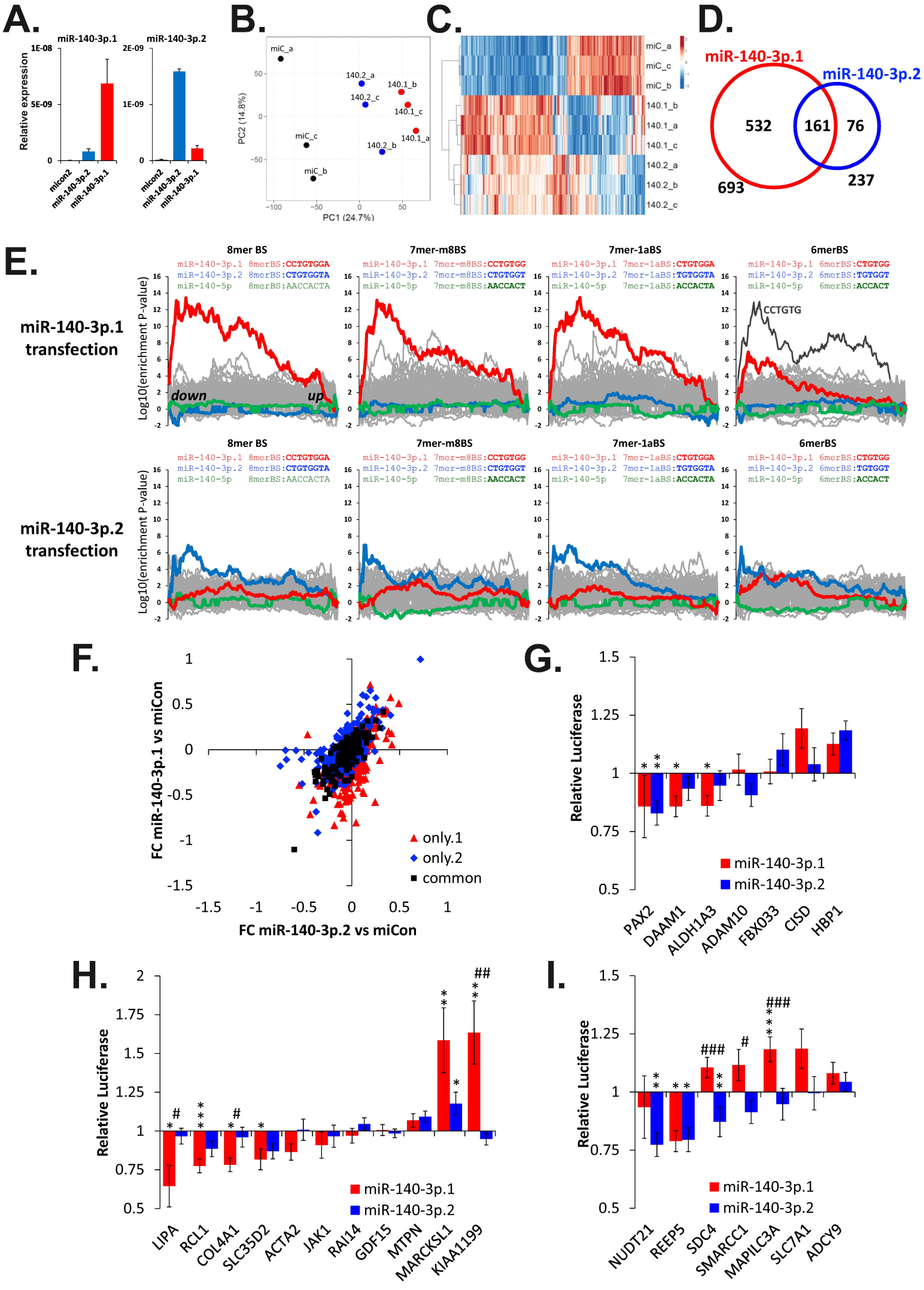
A.
miR-140-3p.1
miR-140-3p.2
Relative expression
1E-08
5E-09
0
2E-09
1E-09
0
micon2
miR-140-3p.2
miR-140-3p.1
B.
PC2 (14.8%)
PC1 (24.7%)
miC_a
140.2_a
140.1_b
140.2_c
140.1_c
140.1_a
miC_c
140.2_b
miC_b
C.
miC_a
miC_c
miC_b
140.1_b
140.1_a
140.1_c
140.2_a
140.2_b
140.2_c
D.
miR-140-3p.1
miR-140-3p.2
532
161
76
693
237
E.
8mer BS
7mer-m8BS
7mer-1aBS
6merBS
miR-140-3p.1 8merBS:CCTGTGGA
miR-140-3p.2 8merBS:CTGTGGTA
miR-140-5p 8merBS:AACCACTA
miR-140-3p.1 7mer-m8BS:CCTGTGG
miR-140-3p.2 7mer-m8BS:CTGTGGT
miR-140-5p 7mer-m8BS:AACCACT
miR-140-3p.1 7mer-1aBS:CTGTGGA
miR-140-3p.2 7mer-1aBS:TGTGGTA
miR-140-5p 7mer-1aBS:ACCACTA
miR-140-3p.1 6merBS:CTGTGG
miR-140-3p.2 6merBS:TGTGGT
miR-140-5p 6merBS:ACCACT
CCTGTG
Log10(enrichment P-value)
down
up
miR-140-3p.1 transfection
miR-140-3p.2 transfection
F.
FC miR-140-3p.1 vs miCon
FC miR-140-3p.2 vs miCon
only.1
only.2
common
G.
Relative Luciferase
miR-140-3p.1
miR-140-3p.2
PAX2
DAAM1
ALDH1A3
ADAM10
FBX033
CISD
HBP1
H.
Relative Luciferase
miR-140-3p.1
miR-140-3p.2
LIPA
RCL1
COL4A1
SLC35D2
ACTA2
JAK1
RAI14
GDF15
MTPN
MARCKSL1
KIAA1199
I.
Relative Luciferase
miR-140-3p.1
miR-140-3p.2
NUDT21
REEP5
SDC4
SMARCC1
MAPILC3A
SLC7A1
ADCY9

Figure 4

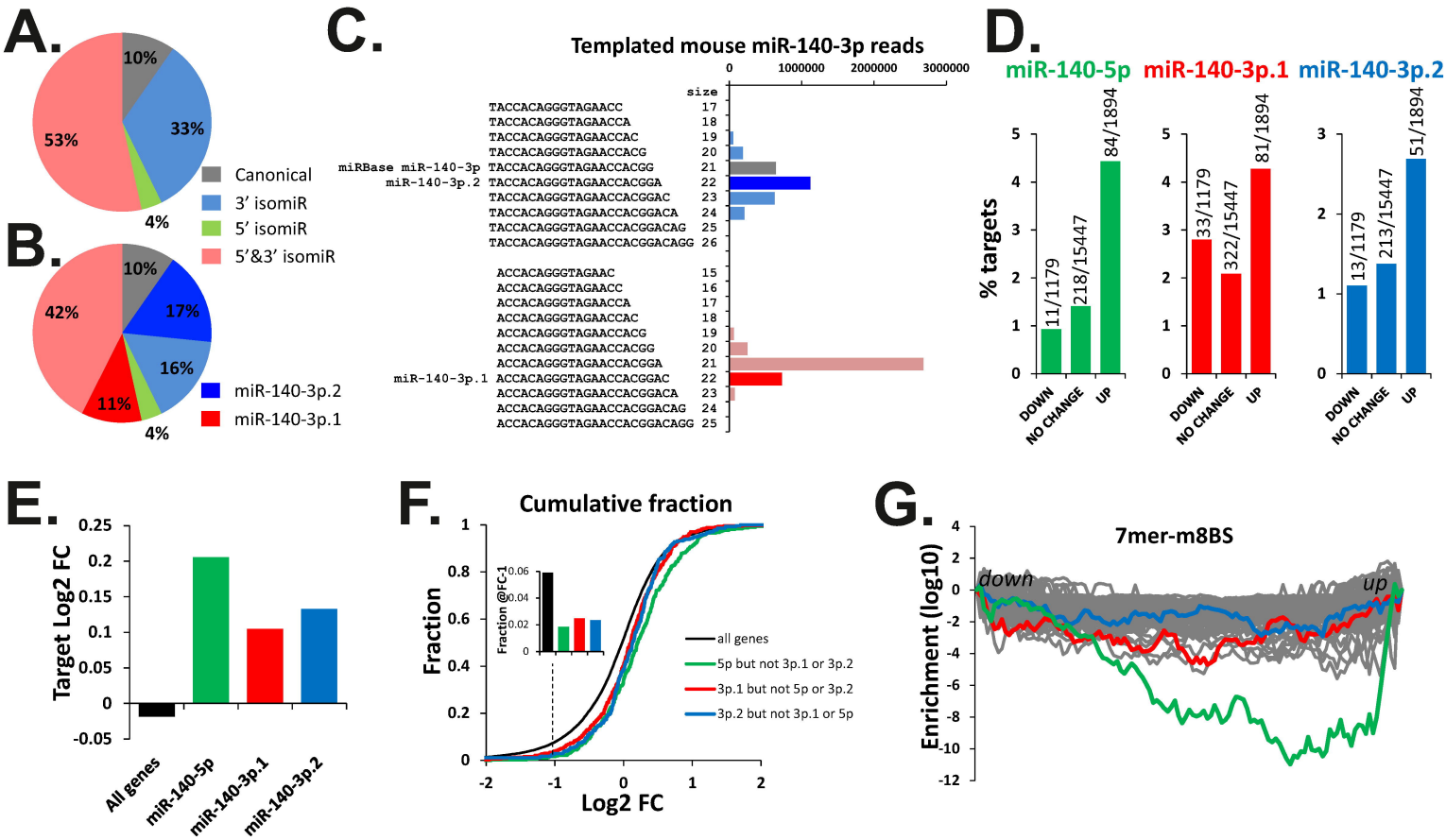
A.
10%
33%
53%
4%
Canonical
3' isomiR
5' isomiR
5'&3' isomiR
B.
10%
17%
16%
11%
4%
42%
miR-140-3p.2
miR-140-3p.1
C.
Templated mouse miR-140-3p reads
0
1000000
2000000
3000000
size
miRBase miR-140-3p
miR-140-3p.2
miR-140-3p.1
TACCACAGGGTAGAACC 17
TACCACAGGGTAGAACCA 18
TACCACAGGGTAGAACCAC 19
TACCACAGGGTAGAACCACG 20
TACCACAGGGTAGAACCACGG 21
TACCACAGGGTAGAACCACGGA 22
TACCACAGGGTAGAACCACGGAC 23
TACCACAGGGTAGAACCACGGACA 24
TACCACAGGGTAGAACCACGGACAG 25
TACCACAGGGTAGAACCACGGACAGG 26
ACCACAGGGTAGAAC 15
ACCACAGGGTAGAACC 16
ACCACAGGGTAGAACCA 17
ACCACAGGGTAGAACCAC 18
ACCACAGGGTAGAACCACG 19
ACCACAGGGTAGAACCACGG 20
ACCACAGGGTAGAACCACGGA 21
ACCACAGGGTAGAACCACGGAC 22
ACCACAGGGTAGAACCACGGACA 23
ACCACAGGGTAGAACCACGGACAG 24
ACCACAGGGTAGAACCACGGACAGG 25
D.
miR-140-5p
miR-140-3p.1
miR-140-3p.2
% targets
11/1179
218/15447
84/1894
33/1179
322/15447
81/1894
13/1179
213/15447
51/1894
DOWN
NO CHANGE
UP

E.
Target Log2 FC
All genes
miR-140-5p
miR-140-3p.1
miR-140-3p.2
F.
Cumulative fraction
Fraction
Fraction @FC-1
Log2 FC
all genes
5p but not 3p.1 or 3p.2
3p.1 but not 5p or 3p.2
3p.2 but not 3p.1 or 5p
G.
7mer-m8BS
Enrichment (log10)
down
up

Figure 5

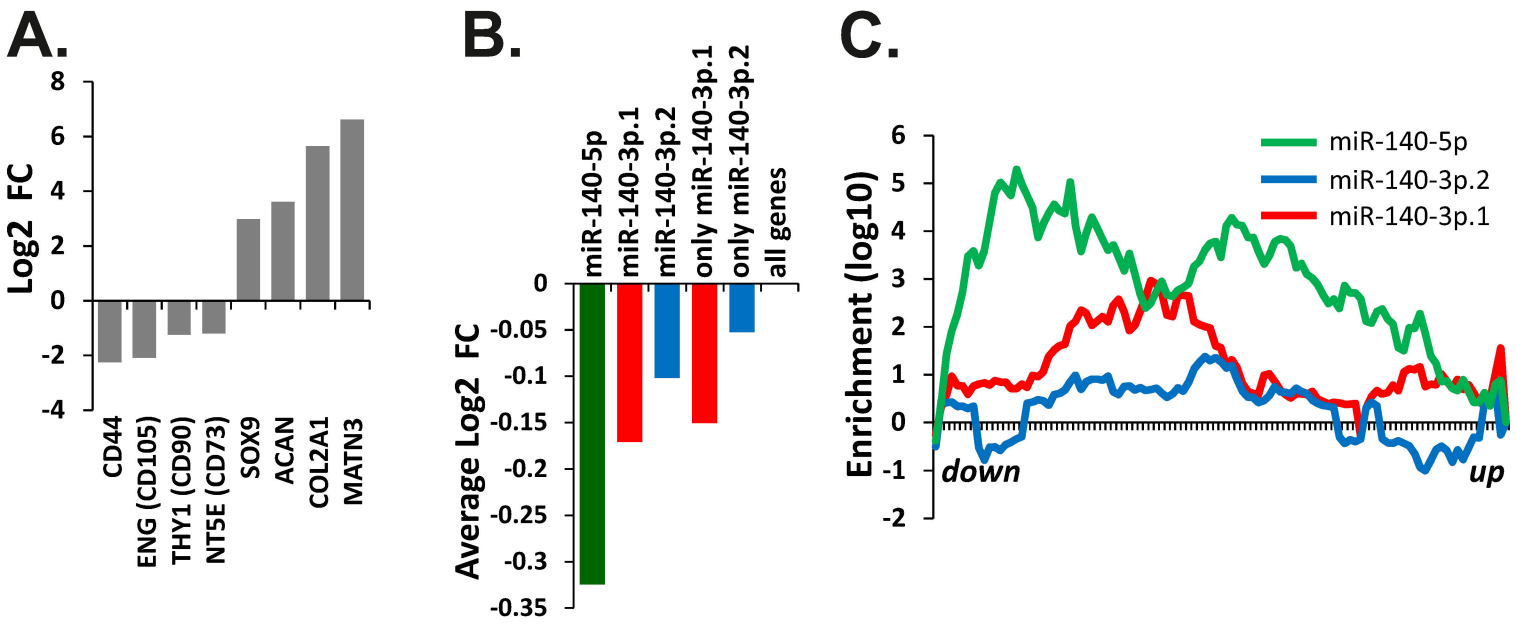
A.
Log2 FC
8
6
4
2
0
-2
-4
CD44
ENG (CD105)
THY1 (CD90)
NT5E (CD73)
SOX9
ACAN
COL2A1
MATN3
B.
Average Log2 FC
0
-0.05
-0.1
-0.15
-0.2
-0.25
-0.3
-0.35
miR-140-5p
miR-140-3p.1
miR-140-3p.2
only miR-140-3p.1
only miR-140-3p.2
all genes
C.
Enrichment (log10)
6
5
4
3
2
1
0
-1
-2
miR-140-5p
miR-140-3p.2
miR-140-3p.1
down
up

Figure 6

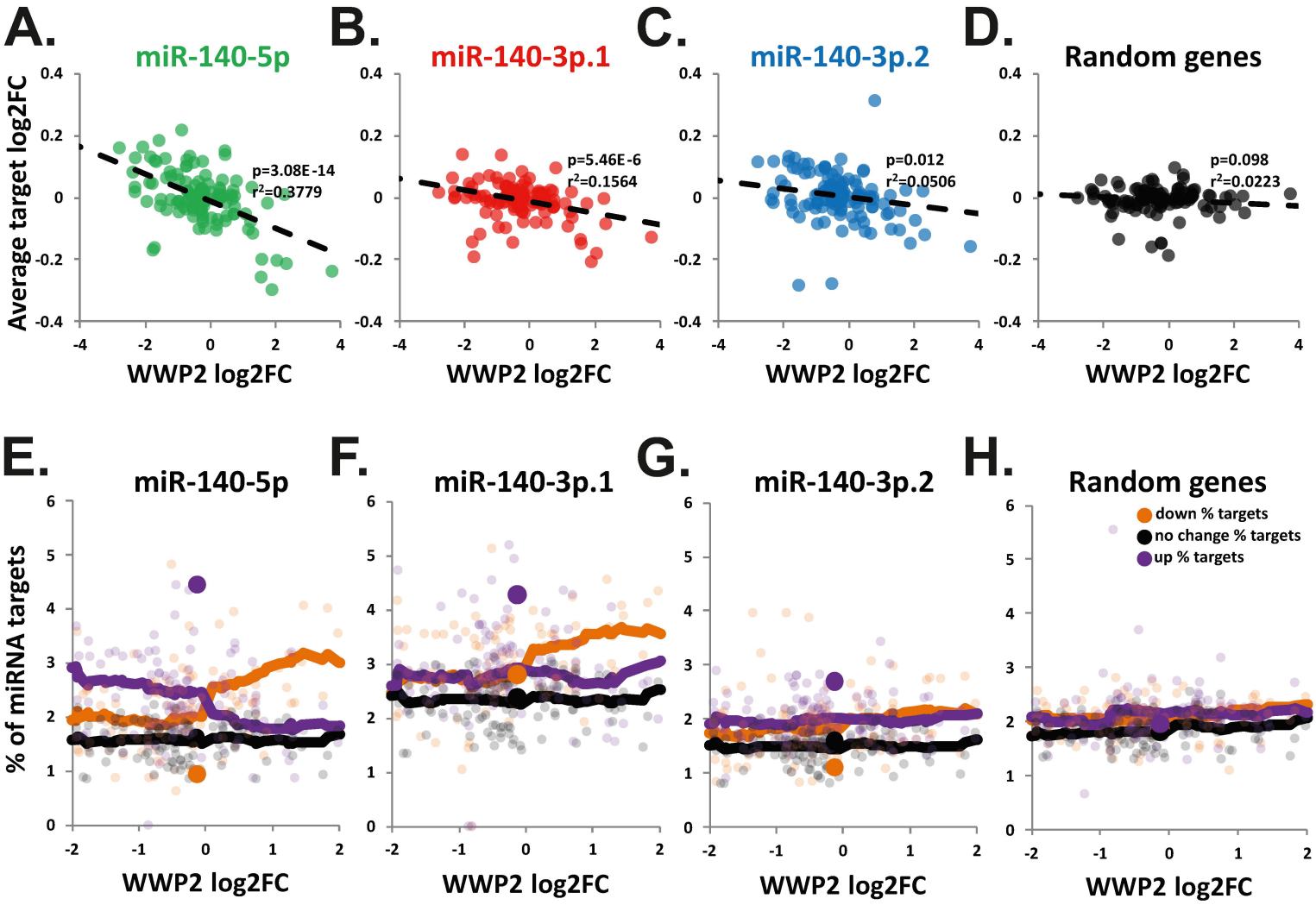
A.
miR-140-5p
p=3.08E-14
r²=0.3779
B.
miR-140-3p.1
p=5.46E-6
r²=0.1564
C.
miR-140-3p.2
p=0.012
r²=0.0506
D.
Random genes
p=0.098
r²=0.0223
Average target log2FC
WWP2 log2FC
E.
miR-140-5p
F.
miR-140-3p.1
G.
miR-140-3p.2
H.
Random genes
down % targets
no change % targets
up % targets
% of miRNA targets
WWP2 log2FC